Journal of Materials Chemistry

Cite this: J. Mater. Chem., 2011, 21, 17754

www.rsc.org/materials

PAPER

Mechanism of capacity fade of MCMB/$Li_{1.1}[Ni_{1/3}Mn_{1/3}Co_{1/3}]_{0.9}O_2$ cell at elevated temperature and additives to improve its cycle life†

Khalil Amine,*[a] Zonghai Chen,[a] Z. Zhang,[a] Jun Liu,[a] Wenquan Lu,[a] Yan Qin,[a] Jun Lu,[a] Larry Curtis[a] and Yang-Kook Sun*[b]

Received 14th April 2011, Accepted 7th September 2011
DOI: 10.1039/c1jm11584g

The performance degradation of graphite/$Li_{1.1}[Ni_{1/3}Mn_{1/3}Co_{1/3}]_{0.9}O_2$ lithium-ion cells at elevated temperature was investigated. The electrochemical data suggest that the migration of dissolved transition metals from the cathode to the anode is the key contributor to the performance degradation. With the help of density function theory calculations, lithium difluoro[oxalato] borate was tested to be an effective electrolyte additive to mitigate the performance degradation of lithium-ion cells. The application of this novel electrolyte additive was found to significantly improve both the life and safety characteristics of graphite/$Li_{1.1}[Ni_{1/3}Mn_{1/3}Co_{1/3}]_{0.9}O_2$ lithium-ion cells.

1. Introduction

New green technologies are urgently needed to reduce fossil fuel consumption in the transportation sector. In this context, worldwide effort is underway to develop plug-in hybrid electric vehicles (PHEVs), hybrid electric vehicles (HEVs), and all-electric vehicles (EVs) that can displace internal combustion vehicles. Lithium-ion batteries which exhibit the highest power and energy density of any existing commercial battery systems, offer many advantages for applications in the transportation sector.[1,2] Among the existing cathode chemistries used in lithium batteries, $LiMn_2O_4$ spinel (LMO)[3–5] and $LiFePO_4$ olivine[6–9] show considerable promise for high-power applications such as HEVs. However, these cathodes offer very limited capacity and thus are not suitable for PHEVs and EVs. The layered oxide materials such as $LiNi_{0.8}Co_{0.1}Mn_{0.1}O_2$ or $LiNi_{0.8}Co_{0.15}Al_{0.05}O_2$ (NCA) offer much higher capacity but exhibit poor calendar life and safety performance. The only commercially available cathode material that has the potential of meeting the PHEV or EV power and energy requirement is $Li_{1.1}[Ni_{1/3}Mn_{1/3}Co_{1/3}]_{0.9}O_2$ (NMC). This cathode material exhibits high capacity of 160 mAh g^{-1} with an average voltage of 3.6 V and powder densities of 2.6 g cc^{-1}. As a result, NMC has the potential of very high energy density, over 200 Wh kg^{-1}. Unlike NCA, which shows poor cycle life because of the high amount of oxidative tetravalent Ni at the fully charged state, charged NMC has a limited amount of tetravalent Ni and thus has the potential of long life and improved safety. In addition, the presence of Mn helps to stabilize this material's crystal structure. Furthermore, the electrode structure based on the NMC cathode remains intact, because no volume change takes place during extensive cycling. However, during cycling at elevated temperature, the full cell with NMC cathode and graphite anode exhibits poor power and cycling performance.

In this paper, we discuss the mechanism behind the power and capacity fade of the cell with NMC cathode and suggest a way of improving the performance by using advanced electrolyte additives, which were developed by means of calculations with quantum modeling and density functional theory.

2. Experimental

Transition metal dissolution

0.1 g $Li_{1.1}[Ni_{1/3}Mn_{1/3}Co_{1/3}]_{0.9}O_2$ cathode material was soaked in 1 mL electrolyte, 1.2 M $LiPF_6$ in EC/EMC (3 : 7 by weight), in a sealed contained at 55 °C for one month. The electrolyte was sampled and analyzed by inductively coupled plasma atomic absorption spectroscopy (ICP-AAS) to determine the concentration of transition metal ions in the electrolyte.

Cycle life test

2032 coin-type full cells using MCMB as the anode, if not specified, were first cycled between 3.0 V and 4.1 V with a constant current of C/10. After the formation cycle, the cells were charged/discharged using a constant current of either C/2 or 1 C between 3.0 V and 4.1 V. High temperature experiments were carried out in a 55 °C oven.

[a]*Electrochemical Technology Program, Chemical Sciences and Engineering Division, Argonne National Laboratory, 9700 South Cass Avenue, Argonne, Illinois, 60439, USA*
[b]*Department of WCU Energy Engineering, Hanyang University, Seoul, 133-791, South Korea*
† Electronic supplementary information (ESI) available. See DOI: 10.1039/c1jm11584g

AC impedance

Lithium-ion cells were first cycled between 3.0 V and 4.1 V with a constant current of C/10 before being constant-voltage charged to 3.85 V. The AC impedance data were collected with an IM 6 electrochemical impedance analyzer using 5 mV stimulating wave. The frequency range for the experiment was between 20 mHz and 1 MHz.

Aging/calendar life test

Lithium-ion cells were first cycled between 3.0 V and 4.1 V with a constant current of C/10 before being constant-voltage charged to 3.85 V and stored in a 55 °C oven. During aging testing, one pair of short high rate pulses (5 C for 3 s) was applied to measure the area specific impedance (ASI) each day. The ASI was determined by the following equation:

$$ASI = \frac{\Delta V}{I} A \quad (1)$$

where ΔV is the voltage difference of the cell before and at the end of the current pulse, I is the current used to measure the ASI, and A is the total surface area of the electrode (either the cathode or anode).

Reference electrode experiment

The lithium-ion cells were slightly modified with two layers of separators sandwiched between the cathode and anode. A reference electrode consisting of micro-sized copper wire coated with a thin layer of Sn was placed between the two separators. Before the experiment, the Sn reference electrode was slightly lithiated to achieve a stable potential. During the ASI measurement, a pair of current pulses was applied, and the potential change of both the cathode and anode was measured against the Li_xSn reference electrode. The ASI was then calculated for the cathode and anode by using eqn (1).

Computational methods

Density functional theory was used for all of the calculations.[10] Geometry optimizations were performed at the B3LYP/631G* level of theory. This was followed by calculation of vibration frequencies (scaled by 0.96) and gas-phase free energies evaluated at 298.15 K. The solvation effects were included by single-point B3LYP/631 + G* calculations using the polarizable continuum model (PCM) with a dielectric constant of 55.7 to mimic a mixture of carbonate electrolytes (25% EC/25% EMC with 50% polycarbonate). In addition, in some cases we carried out B3LYP calculations with a larger basis set, 6311 + G (3df,2p) at the B3LYP/6-31G* geometries. An electron solvation free energy of −1.63 eV in water was assumed.[11]

3. Results and discussion

Fig. 1 shows normalized capacity *versus* cycle number for mesocarbon microbead (MCMB)/NMC cells at 25 and 55 °C. Testing was done at a constant current density of 1 C-rate cycled between 3.0 and 4.1 V. The cell cycled at 25 °C showed no capacity fade after 80 cycles, while the cell cycled at 55 °C lost more than 28% capacity. To investigate the origin of the

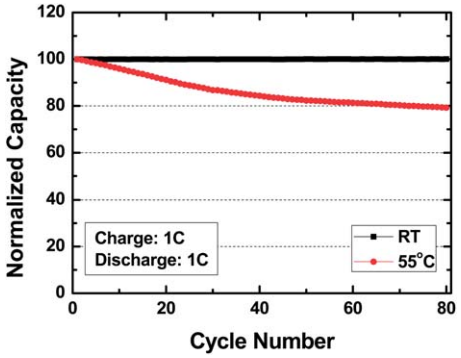

Fig. 1 Normalized discharge capacity *vs.* cycle number of MCMB/$Li_{1.1}[Ni_{1/3}Mn_{1/3}Co_{1/3}]_{0.9}O_2$ cell cycled at 1 C-rate between 3.0 and 4.0 V at room temperature and 55 °C.

significant capacity fade of the MCMB/NMC cell at elevated temperature, we measured its area specific impedance during cycling at 55 °C by using a specially designed Li-Sn reference electrode technique.[12] The changes in the ASI of the cathode, the anode, and the cell over more than 400 cycles is shown in Fig. 2. The cathode impedance did not change during cycling, while the anode impedance increased significantly and closely matched that of the full cell. This result clearly shows that the carbon anode is responsible for the overall cell capacity and power fade. A similar mechanism was also observed in tests with $LiMn_2O_4$/graphite cells.[3,5,13,14] In this case, the Mn ion dissolves from the surface of the cathode at high temperature, migrates to the anode, and reduces to the active metallic form, which causes the breakdown of the solid-electrolyte interface (SEI) and leads to an increase of the anode interfacial impedance.

To confirm the negative effect of Mn^{2+} dissolution on the SEI layer at the carbon anode, we investigated the cycle life of a $Li_4Ti_5O_{12}$ (LTO)/NMC cell together with a MCMB/NMC cell, and the results are shown in Fig. 3. Unlike the conventional carbon anode, which forms an SEI layer at 0.8–0.9 V (*vs.* Li/Li^+) during charging, the spinel (LTO) forms no SEI due to its flat and high potential around 1.5 V (*vs.* Li/Li^+).[15–17] The LTO/NMC cell showed almost no capacity fade after 180 cycles under these aggressive test conditions, while the MCMB/NMC cell lost more than 27% capacity after only 90 cycles. Therefore, we believe that the capacity fade in the NMC/MCMB cell is caused by the

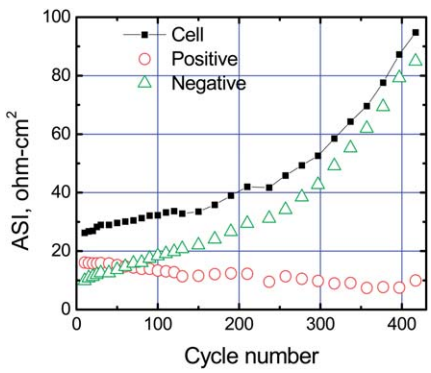

Fig. 2 Area specific impedance (ASI) *vs.* cycle number for MCMB/$Li_{1.1}[Ni_{1/3}Mn_{1/3}Co_{1/3}]_{0.9}O_2$ cell.

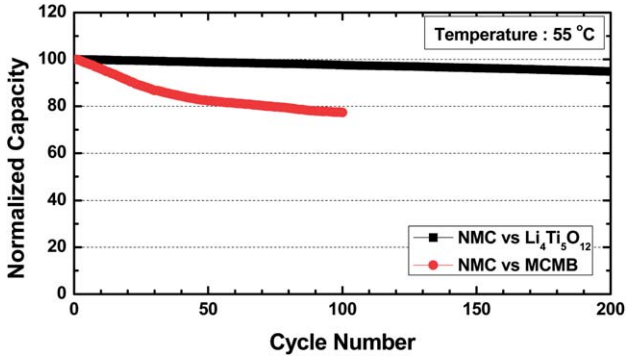

Fig. 3 Normalized discharge capacity *vs.* cycle number of MCMB/$Li_{1.1}[Ni_{1/3}Mn_{1/3}Co_{1/3}]_{0.9}O_2$ and $Li_4Ti_5O_{12}/Li_{1.1}[Ni_{1/3}Mn_{1/3}Co_{1/3}]_{0.9}O_2$ cells cycled at 1 C-rate between 3.0 and 4.0 V at 55 °C.

dissolution of the transition metals, which eventually reduces to active metallic form at the surface of the MCMB anode and compromises the SEI film, leading to the observed increase in the anode impedance (Fig. 2). Fig. 4 shows the concentration of dissolved Ni, Mn, and Co, measured by inductively coupled plasma atomic absorption spectroscopy, after exposing the NMC cathode to the electrolyte for one month at 55 °C. The dissolved amounts of Ni, Co, and Mn were measured to be 15, 13, and 15.3 ppm, respectively. While tetravalent Mn is not involved in the electrochemical reaction, this ion showed the greatest amount of dissolution because of Mn leaching due to HF at the cathode surface. In order to verify the possibility of transition metal migration to the anode, a lithium-ion button cell using $Li_{1.1}[Mn_{1/3}Ni_{1/3}Co_{1/3}]_{0.9}O_2$ as the cathode and MCMB as the anode was assembled for the aging test. The electrolyte used was 1.2 M $LiPF_6$ in mixture solvent of EC/EMC (3 : 7 by weight). The cell was initially cycled between 3.0 V and 4.1 V for 2 cycles with a constant current of C/10 before being constant-voltage charged to 4.1 V. The charged cell was then stored in a 55 °C oven for 3 weeks. After aging, the cell was fully discharged, and was disassembled to harvest the aged MCMB anode. The anode was then rinsed with dimethyl carbonate (DMC) for three times to remove electrolyte residues. After drying in a vacuum, the dried MCMB film was characterized with X-ray photoelectron spectroscopy (XPS), to probe the existence of transition metal on MCMB anode. Small amount of Ni was detected with XPS, the signal for Mn was only about the level of noise and Co was not detected at current sensitivity level of XPS (see Figure 1S†).

The most promising approach to mitigate the negative impact of transition metal dissolution on the carbon anode is formation of a more stable artificial SEI by using functional electrolyte additives, thereby improving the capacity retention of lithium-ion cells.[18] Among the additives reported in the literature, lithium bis(oxalato)borate (LiBOB) has been recognized as an effective electrolyte additive to form a stable solid electrolyte interface (SEI). However, this additive leads to very high interfacial impedance and therefore power loss. Hence, we carried out computational studies for such additives. In these studies we first investigated the reduction of the anions of two borate-based salts, LiBOB and lithium difluoro(oxalato)borate (LiDFOB), and three possible products that might result from the reduction. For LiBOB these three products include (a) opening of one oxalate ring *via* breaking a B–O bond, (b) decomposition by breaking two B–O bonds to form C_2O_4 and BC_2O_4 anions, and (c) decomposition by breaking a B–O bond and a C–O bond on the same ring to form C_2O_3 and OBC_2O_4 anions, as shown in Fig. 5. We found that in terms of free energies (relative to the BOB anion plus an electron) (a) is exothermic by 0.6 eV, (b) is endothermic by 2.7 eV, and (c) is exothermic by 0.5 eV. Thus, (a) and (c) are possible reduction products for LiBOB.

For DFBOB, the three products considered include (a) opening of the oxalate ring *via* breaking a B–O bond, (b) decomposition by breaking two B–O bonds to form C_2O_4 and BF_2 anions, and (c) decomposition by breaking a B–O bond and a C–O bond on the same ring to form C_2O_3 and OBF_2 anions, as shown in Fig. 6. The latter decomposition was proposed by Xiao *et al.*[19] We found that in terms of free energies (relative to the DFOB anion plus an electron) (a) is endothermic by 1.0 eV, (b) is endothermic by 2.7 eV, and (c) is exothermic by 0.3 eV. Thus, for DFOB the calculations suggest that the only viable products are decomposition to form C_2O_3 and OBF_2.

Based on the results for the reduction products, we investigated possible polymerization products resulting from reduction of LiBOB and LiDFOB. For LiBOB we considered

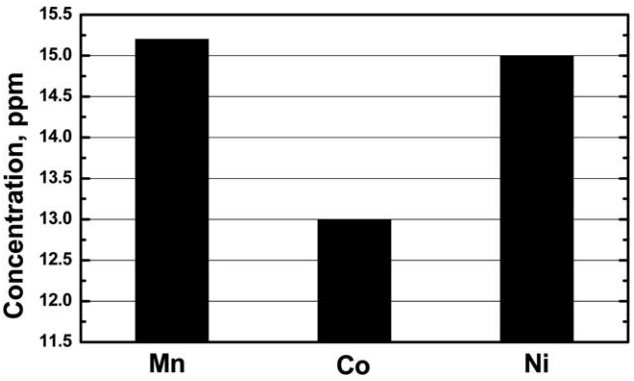

Fig. 4 Concentration of Ni, Co, and Mn in electrolyte of Li/$Li_{1.1}[Ni_{1/3}Mn_{1/3}Co_{1/3}]_{0.9}O_2$ cells after one month at 55 °C.

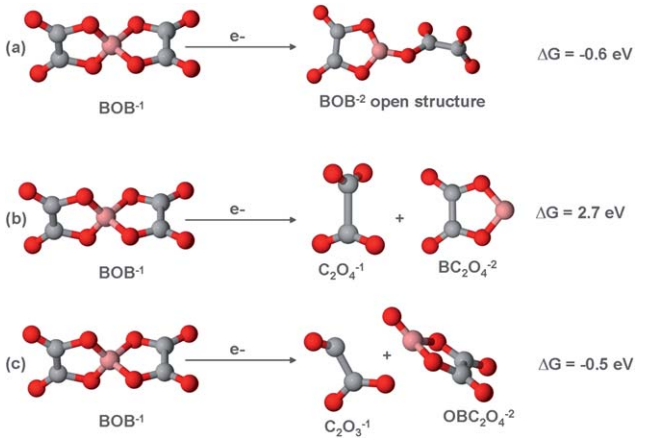

Fig. 5 Structures in BOB anion reduction reactions (B = pink, O = red, and C = gray).

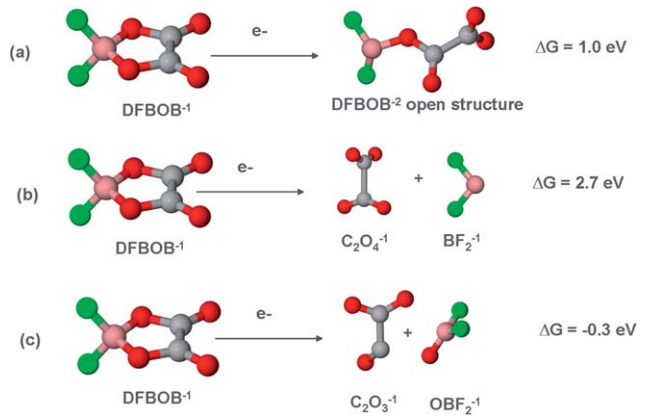

Fig. 6 Structures in DFOB anion reduction reactions (B = pink, F = green, O = red, and C = gray).

polymerization of the BOB dianion having an open ring (see Fig. 5) and the decomposition product OBC_2O_4 anion. For the BOB open ring, our density functional calculations showed dimerization was slightly exothermic, but trimerization was endothermic. In contrast, the calculations showed the free energies of formation of dimers, trimers, and tetramers of the OBC_2O_4 anion are exothermic. There are numerous possible structures for the n-mers of OBC_2O_4, and the energetically most favorable ones are shown Fig. 7. They exhibit a three-dimensional structure and are energetically favorable by 1.4–1.6 eV. For LiDFOB we considered polymerization of the OBF_2 anion decomposition product since this was the favorable reduction product, as discussed above. The dimers, trimers, and tetramers are exothermic by about 0.2–0.4 eV and have linear structures, as also shown in Fig. 7. Based on the studies of these n-mers we concluded that appropriate modification of LiBOB can have a dramatic effect on the polymerization structures formed. The calculations suggest that the fluorine termination of LiDFOB prevents three-dimensional polymerization structures. Therefore, we can expect the artificial SEI layer formed with LiDFOB to be thinner than that formed with LiBOB, and much lower interfacial impedance is expected for the LiDFOB electrolyte additive. This prediction was proven experimentally by studying the AC impedance of MCMB/NMC cells with LiBOB and LiDFOB as electrolyte additives.

Fig. 8 shows the AC impedance of an MCMB/NMC cell using 2.0 wt% LiDFOB as electrolyte additive. Fig. 8 also shows the AC impedance data for the cells without additive and with 2.0 wt% LiBOB for comparison. It is clear that the addition of 2.0 wt% LiDFOB to the electrolyte only slightly increased the interfacial impedance of the lithium-ion cells, and that the impedance increase was much smaller than that of the cell with 2.0 wt% LiBOB. This finding confirms that the crosslinking reaction between the polymer chains is responsible for the high interfacial impedance of LiBOB additive as predicted by density functional theory.

Fig. 9 shows the capacity retention of an 18650 cell using MCMB as the anode and NMC as the cathode. This cell was operated for 1000 cycles at 55 °C between 3.0 V and 4.1 V with a constant current of 0.8 A (1 C-rate). The electrolyte was 1.2 M $LiPF_6$ in EC/EMC (3 : 7 by weight) with 2 wt% LiDFOB. The cell was designed for high power application with a thin electrode coating, and the initial capacity was about 800 mAh. Even after testing at 55 °C for 1000 cycles, the cell with 2 wt% LiDFOB still had 78% capacity retention. By contrast, the cell without electrolyte additive lost about 25% reversible capacity after 80 cycles (see Fig. 1).

Fig. 10 shows the ASI of two 18650 cells during calendar life testing at 55 °C. One of the cells was prepared with 2.0 wt% LiDFOB as the electrolyte additive, and the other had no additive. Both cells were constant-voltage charged to 3.85 V before being stored in an oven at 55 °C. During the calendar life test, a pair of 5 C (4.0 A) current pulses for 3 s was applied each day to measure the cell ASI. Fig. 10 shows that the initial ASI of both cells was about 11 $\Omega \cdot cm^2$. The ASI of the cell without additive increased to 22 $\Omega \cdot cm^2$ in about 80 days aging, while the cell with 2 wt% LiDFOB showed a small ASI increase, to about 12 $\Omega \cdot cm^2$ (about 10% increase), after 80 days of aging.

The performance improvement shown in Fig. 10 can be explained by the formation of a stable artificial SEI layer on the anode surface that protects the graphite from the effect of Mn, Ni, and Co dissolution. Based on the same philosophy, this stable artificial SEI layer can also act as a physical barrier to suppress

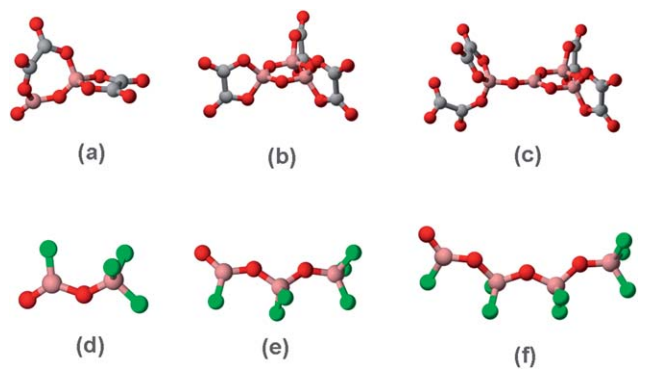

Fig. 7 Structures of (a) dimers, (b) trimers, and (c) tetramers of decomposition species of LiBOB (OBC_2O_4) and (d) dimers, (e) trimers, and (f) tetramers of LiDFOB (OBF_2) (B = pink, F = green, O = red, and C = gray).

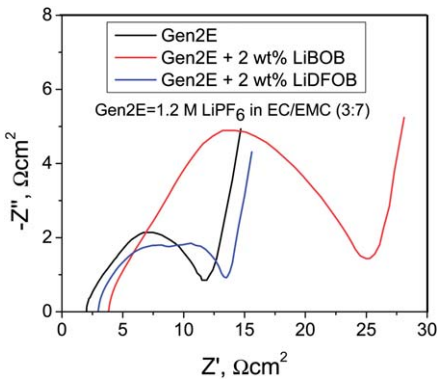

Fig. 8 AC impedance of MCMB/$Li_{1.1}[Ni_{1/3}Mn_{1/3}Co_{1/3}]_{0.9}O_2$ cells using different electrolytes, showing the advantage of LiDFOB over LiBOB. The baseline electrolyte is 1.2 M $LiPF_6$ in ethylene carbonate (EC): ethyl methyl carbonate (EMC) (3 : 7 by weight).

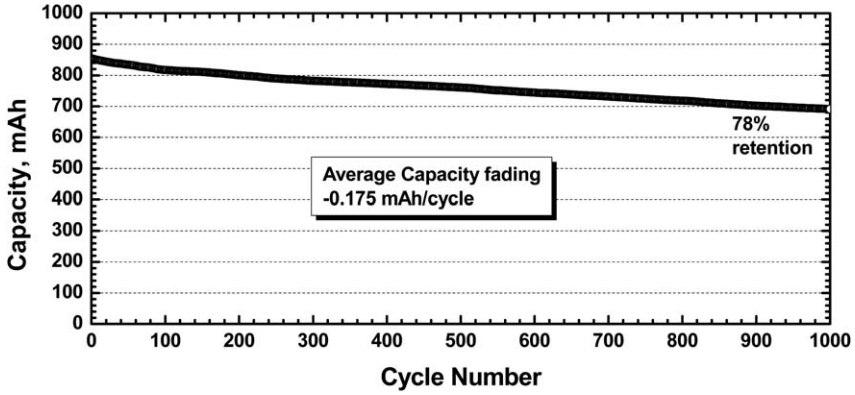

Fig. 9 Capacity retention of 18650 cell using MCMB/$Li_{1.1}[Ni_{1/3}Mn_{1/3}Co_{1/3}]_{0.9}O_2$ electrodes during high-temperature (55 °C) cycling test at 1C rate. The electrolyte used was 1.2 M $LiPF_6$ in EC/EMC (3 : 7 by weight) with 2.0 wt% LiDFOB.

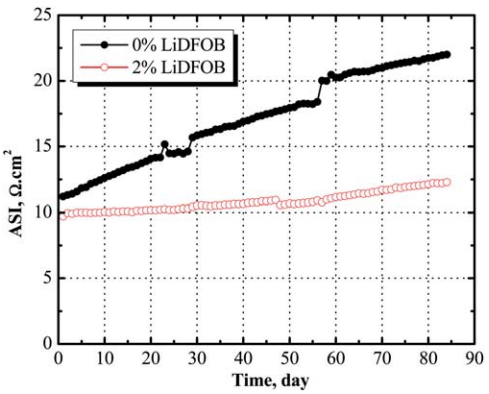

Fig. 10 ASI of 18650 cell using MCMB/$Li_{1.1}[Ni_{1/3}Mn_{1/3}Co_{1/3}]_{0.9}O_2$ with and without LiDFOB additive during aging tests at 55 °C and 3.85 V.

the chemical reaction between the lithiated graphite and the non-aqueous electrolyte. Therefore, we can also expect improved thermal stability of lithiated graphite with the presence of non-aqueous electrolytes.

Fig. 11 illustrates the connection between the SEI stability and the thermal stability of lithiated graphite in non-aqueous electrolyte. The differential scanning calorimetry (DSC) profile of the delithiated graphite (with only SEI layer on the surface and no lithium in the graphite) showed a small exothermal peak at about 100 °C, which we attributed to the thermal decomposition of the SEI layer. Fig. 11 also shows the DSC profile for a sample of lithiated graphite and equivalent amount of non-aqueous electrolyte (1.2 M $LiPF_6$ in EC/EMC, 3 : 7 weight ratio), where the onset temperature for the exothermal reaction is identical to that of SEI decomposition. After the SEI decomposition, the heat flow continued to increase until about 145 °C, at which temperature a constant heat flow was measured. We believe that the decomposition of the SEI layer led to the direct exposure of lithiated graphite to non-aqueous electrolyte, resulting in the continuous but slow reaction of the lithiated graphite with electrolyte. In some cases, the heat generated from this continuous process can be enough to heat the cell to a higher temperature and trigger a thermal runaway reaction of lithium-ion cells.[20] Therefore, a more stable SEI layer can delay the direct exposure of lithiated graphite to electrolyte and enhance the safety of lithium-ion cells. Fig. 12 shows the positive effect of LiDFOB additive on the thermal stability of lithiated graphite, pushing the onset temperature of the exothermal reaction up to above 160 °C. This occurs because the activation energy for breaking the new artificial SEI caused by the polymerization of LDFOB is very high, and this layer requires more energy to be broken down.

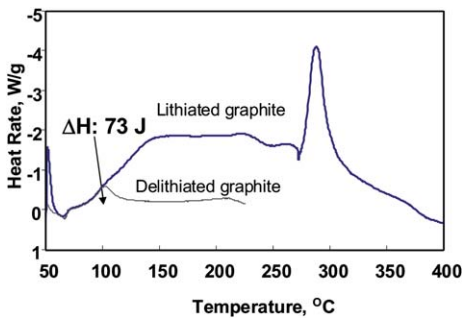

Fig. 11 DSC profile of lithiated and delithiated graphite to illustrate the importance of SEI stability to the safety of lithiated graphite.

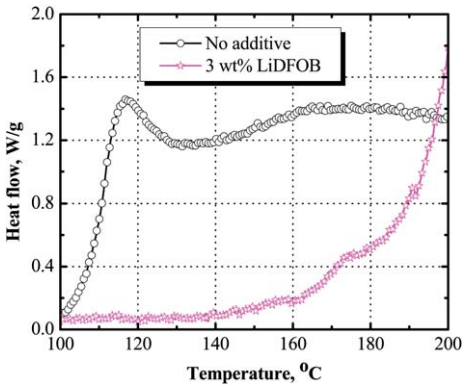

Fig. 12 DSC profile of lithiated MCMB with the presence of non-aqueous electrolyte, showing that LiDFOB additive provides a more stable artificial SEI layer that would delay the exothermal reaction between lithiated MCMB and non-aqueous electrolyte.

4. Conclusions

The mechanism of power and energy fade in the promising NMC-based cell was attributed to the dissolution of Mn, Ni, and Co ions. These metal ions migrate from the cathode to the anode and reduce to a metallic state at the SEI. The metal or metal alloy deposited on the surface of the graphite anode has a detrimental effect on the stability of the SEI. Lithium difluoro[oxalato] borate was demonstrated, from theoretical calculations and cell tests, to be an effective electrolyte additive, suppressing the effect of the metal deposition and thereby significantly extending the cycle life of lithium-ion cells without sacrificing the rate capability. Moreover, this novel electrolyte additive also enhances the thermal stability of lithiated graphite in the presence of non-aqueous electrolytes.

Acknowledgements

Research funded by U.S. Department of Energy, FreedomCAR and Vehicle Technologies Office. Argonne National Laboratory is operated for the U.S. Department of Energy by UChicago Argonne, LLC, under contract DE-AC02-06CH11357. This work was also supported by the Human Resources Development of the Korea Institute of Energy Technology Evaluation and Planning (KETEP) grant funded by the Korea government Ministry of Knowledge Economy (No. 20104010100560) and the Korea Research Foundation Grant funded by the Korean Government (MEST) (KRF-2008-220-D00035).

References

1 J.-M. Tarascon and M. Armand, *Nature*, 2001, **414**, 359.
2 T. H. Bradley and A. A. Frank, *Renewable Sustainable Energy Rev.*, 2009, **13**, 115.
3 A. Blyr, C. Sigala, G. Amatucci, D. Guyomard, Y. Chabre and J.-M. Tarascon, *J. Electrochem. Soc.*, 1998, **145**, 194.
4 D. D. MacNeil, T. D. Hatchard and J. R. Dahn, *J. Electrochem. Soc.*, 2001, **148**, A663.
5 K. Amine, J. Liu, S. Kang, I. Belharouak, Y. Hyung, D. Vissers and G. Henriksen, *J. Power Sources*, 2004, **129**, 14.
6 A. K. Padhi, K. S. Nanjundaswamy and J. B. Goodenough, *J. Electrochem. Soc.*, 1997, **144**, 1188.
7 S. Y. Chung, J. T. Bloking and Y. M. Chiang, *Nat. Mater.*, 2002, **1**, 123.
8 Y. J. Lee, H. Yi, W. J. Kim, K. Kang, D. S. Yun, M. S. Strano, G. Ceder and A. M. Belcher, *Science*, 2008, **324**, 1051.
9 S. W. Oh, S.-T. Myung, S.-M. Oh, K. H. Oh, K. Amine, B. Scrosati and Y.-K. Sun, *Adv. Mater.*, 2010, **22**, 4842.
10 M. J. Frisch, G. W. Trucks, H. B. Schlegel, G. E. Scuseria, M. A. Robb, J. R. Cheeseman, J. A. Montgomery, J. T. Vreven, K. N. Kudin, J. C. Burant, J. M. Millam, S. S. Iyengar, J. Tomasi, V. Barone, B. Mennucci, M. Cossi, G. Scalmani, N. Rega, G. A. Petersson, H. Nakatsuji, M. Hada, M. Ehara, K. Toyota, R. Fukuda, J. Hasegawa, M. Ishida, T. Nakajima, Y. Honda, O. Kitao, H. Nakai, M. Klene, X. Li, J. E. Knox, H. P. Hratchian, J. B. Cross, C. Adamo, J. Jaramillo, R. Gomperts, R. E. Stratmann, O. Yazyev, A. J. Austin, R. Cammi, C. Pomelli, J. W. Ochterski, P. Y. Ayala, K. Morokuma, G. A. Voth, P. Salvador, J. J. Dannenberg, V. G. Zakrzewski, S. Dapprich, A. D. Daniels, M. C. Strain, O. Farkas, D. K. Malick, A. D. Rabuck, K. Raghavachari, J. B. Foresman, J. V. Ortiz, Q. Cui, A. G. Baboul, S. Clifford, J. Cioslowski, B. B. Stefanov, G. Liu, A. Liashenko, P. Piskorz, I. Komaromi, R. L. Martin, D. J. Fox, T. Keith, M. A. Al-Laham, C. Y. Peng, A. Nanayakkara, M. Challacombe, P. M. W. Gill, B. Johnson, W. Chen, M. W. Wong, C. Gonzalez, and J. A. Pople, *Gaussian 03, Revision C.02*, Gaussian Inc., Wallingford CT, 2004.
11 Y. Tabata, ed., *RC Handbook of Radiation Chemistry*, CRC Press, Boca Raton, FL, 1991, pp. 335.
12 D. P. Abraham, J. Liu, C. H. Chen, Y. E. Hyung, M. Stoll, N. Elsen, S. MacLaren, R. Twesten, R. Haasch, E. Sammann, I. Petrov, K. Amine and G. Henriksen, *J. Power Sources*, 2003, **119–121**, 511.
13 S. Komaba, N. Kumagai and Y. Kataoka, *Electrochim. Acta*, 2002, **47**, 1229.
14 S. Komaba, B. Kaplan, T. Ohtsuka, Y. Kataoka, N. Kumagai and H. Groult, *J. Power Sources*, 2003, **119–121**, 378.
15 K. M. Colbow, J. R. Dahn and R. R. Haering, *J. Power Sources*, 1989, **26**, 397.
16 I. Belharouak, Y.-K. Sun, W. Lu and K. Amine, *J. Electrochem. Soc.*, 2007, **154**, A1083.
17 K. Amine, I. Belharouak, Z. Chen, T. Taison, H. Yumoto, N. Ota, S.-T. Myung and Y.-K. Sun, *Adv. Mater.*, 2010, **22**, 3052.
18 Z. H. Chen, W. Q. Lu, J. Liu and K. Amine, *Electrochim. Acta*, 2006, **51**, 3322.
19 A. Xiao, Li. Yang, B. L. Lucht, S.-H. Kang and D. P. Abraham, *J. Electrochem. Soc.*, 2009, **156**, A318.
20 J. W. Jiang, H. Fortier, J. N. Reimers and J. R. Dahn, *J. Electrochem. Soc.*, 2004, **151**, A609.